

# Chemical Composition of Fresh and Aged Asphalt-Related Organic Aerosols: From Ambient Observations to Laboratory Experiments

Peeyush Khare, Jo Machesky, Leah Williams, Mackenzie Humes, Edward C. Fortner, Manjula Canagaratna, Jordan E. Krechmer, Andrew T. Lambe, Albert A. Presto, and Drew R. Gentner\*



Cite This: <https://doi.org/10.1021/acsestair.4c00193>



Read Online

ACCESS |



Metrics & More



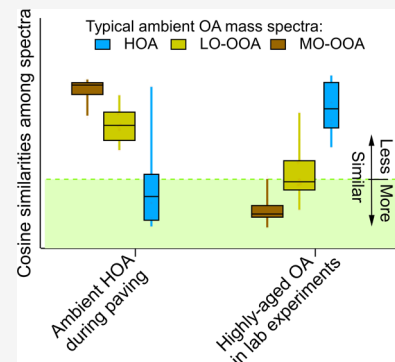
Article Recommendations



Supporting Information

**ABSTRACT:** Asphalt-related emissions are an understudied source of reactive organic compounds with the potential to form organic aerosol (OA). Ambient aerosol mass spectrometry (AMS) measurements of asphalt-related aerosols near a month-long road paving project showed enhanced ambient OA concentrations with a mix of primary and secondary OA signatures. For comparison, gas-phase emissions from real-world road asphalt samples at application (e.g., 140 °C) and in-use (e.g., 60 °C) temperatures were injected into an environmental chamber and an oxidation flow reactor to simulate varying degrees of oxidative aging while measuring their gas- and aerosol-phase oxidation products. Secondary OA formation was observed via both self-nucleation and condensation, with chemical properties dependent on asphalt temperature and reaction conditions. The chemical composition of less-aged asphalt-related OA observed in outdoor and laboratory measurements was similar to OA from other petrochemical-based sources and hydrocarbon-like OA source factors observed via AMS in previous urban studies. The composition of aged OA varied with the degree of oxidation, similar to oxidized OA factors observed in ambient air. Taken together, these field and laboratory observations suggest that contributions to urban OA during and after application may be challenging to deconvolve from other traditional sources in ambient measurements.

**KEYWORDS:** Road paving, intermediate- and semivolatile organic compounds, volatile chemical products, organic aerosol, time-of-flight aerosol mass spectrometry



## 1. INTRODUCTION

Airborne fine-mode particulate matter ( $PM_{2.5}$ ) is largely composed of organic and inorganic aerosol that play important roles in air quality and human health. Organic aerosol (OA) now represents a dominant fraction of U.S.  $PM_{2.5}$ <sup>1</sup> and includes both primary organic aerosol (POA) that is directly emitted and secondary organic aerosol (SOA) that forms via atmospheric oxidation of reactive gas-phase precursors.<sup>2,3</sup> These precursors include volatile (VOCs), intermediate volatile (IVOCs), and semivolatile organic compounds (SVOCs) that are emitted from a diverse mix of anthropogenic and biogenic sources with varying and uncertain contributions to urban SOA.<sup>4–10</sup>

Recent estimates suggest that SOA production from anthropogenic emissions of VOCs-SVOCs from noncombustion-related sources (e.g., volatile chemical products) now exceed annual SOA contributions from on-road gasoline and diesel vehicles in developed cities.<sup>5,11–13</sup> Asphalt is one urban source of I/SVOCs, which are important SOA precursors, with widespread urban use and emissions that can occur throughout its material lifecycle.<sup>5,14–18</sup> Yet, its emissions can vary considerably depending on material properties, application methods, usage, age, and geographically varying environmental factors (e.g., summertime surface temperatures).<sup>5,19</sup>

Several prior studies have estimated volatile content in asphalt via mass spectrometry and gravimetric techniques, and emissions of methane, carbon monoxide and other bulk VOCs, polycyclic aromatic hydrocarbons (PAHs), and unspiciated lower volatility compounds (e.g., SVOCs) have also been shown.<sup>11,20–27</sup> Furthermore, the impact of asphalt-related emissions on air quality has been investigated in ambient, laboratory and modeling studies.<sup>14,28–30</sup> Notable examples include a recent U.S. nationwide  $PM_{2.5}$  modeling effort with updated source profiles including I/SVOCs,<sup>14</sup> long-term emissions estimations for samples collected in France and the U.S.,<sup>19,29,30</sup> and molecular-level investigations of asphalt/asphaltene oxidation from solar exposure.<sup>26,31</sup> Some occupational exposure studies have also investigated short-term, near-source exposure of construction workers to ambient hot-mix paving emissions with a focus on bulk particulate matter concentrations and select PAHs.<sup>32–34</sup> All of these varied

**Received:** August 9, 2024

**Revised:** February 28, 2025

**Accepted:** February 28, 2025

measurements identify asphalt as a non-negligible source of reactive organic compounds. The chemical composition and properties of OA resulting from asphalt-related emissions is not well established from either real-world ambient observations<sup>35</sup> or laboratory studies, especially in comparison to other typical urban sources (e.g., gasoline and diesel exhaust).

Laboratory oxidation chambers and flow reactors (OFRs) simulate atmospheric chemical processes with typical atmospheric oxidants (i.e., OH, NO<sub>3</sub>, O<sub>3</sub>) to simulate SOA formation from single reactive precursors or mixtures.<sup>36–41</sup> While larger Teflon-lined chambers generally simulate short-term aging (6–10 h) with atmospherically relevant oxidant concentrations, OFRs can perform multiday aging in minutes with high levels of oxidant exposure. Both have been used widely with complex precursors from other sources that vary in composition and magnitude with time (e.g., evaporative emissions from crude oil, ambient air, vehicle exhaust).<sup>42–48</sup>

The overall objective of this study was to use a combination of ambient and laboratory observations to examine the chemical composition of asphalt-related OA with varying degrees of atmospheric oxidation. Ambient measurements in the vicinity of a 1-month long road paving event in Billerica, MA, were compared with laboratory experiments simulating short- and longer-term atmospheric aging to examine the chemical composition of the OA formed from asphalt-related emissions at application and elevated summertime in-use temperatures. Lastly, we compared the chemical composition of our ambient and lab-generated asphalt-related OA to the OA produced from diverse sources in prior laboratory experiments and also with well-established ambient OA factors from previous studies in urban areas.

## 2. MATERIALS AND METHODS

**2.1. Ambient Aerosol Chemical Composition Measurements.** Measurements of ambient submicrometer particle chemical composition and size were performed at Aerodyne Research, Inc. using a high-resolution time-of-flight aerosol mass spectrometer (HR-ToF-AMS, Aerodyne, SN 215-122). The measurements occurred during 1–26 August 2014, which coincided with nearby asphalt-paving activities, and also during 27 August–20 September 2020 under routine conditions without paving. Ambient air was sampled at 3 L min<sup>-1</sup> through a 2.5 μm cut cyclone on an elevated outdoor platform outside of the Aerodyne Research Facility of 45 Manning Rd., Billerica, MA (42.53, -71.27, 60 m a.s.l.), located ~200 m east of a major freeway (US Route 3; see Figure S1).

The AMS sampled particles through a 100 μm critical orifice and a standard aerodynamic lens that transmits particles with vacuum aerodynamic diameters in the approximately 70 nm to 700 nm size range ( $d_{va}$ ),<sup>49</sup> forming a focused particle beam that is transmitted into the detection region. Here, the non-refractory species are flash vaporized upon impact with a hot surface (600 °C). The particle vapor was ionized using electron impact ionization (70 eV) and detected by the time-of-flight mass spectrometer.<sup>50</sup> Particle size (particle time-of-flight, pToF) data was determined from the particle flight time in the vacuum chamber after passing through a chopper.

Providing baseline measurements over a longer time period, additional particle chemical composition measurements were acquired for multiple days at a time from June 2013 to December 2014 using various aerosol chemical speciation monitors (ACSMs). The ACSM operates on the same principle as the AMS but without any particle size differ-

entiation below its PM<sub>1</sub> size cut. These instruments included either a quadrupole mass spectrometer or a unit mass resolution time-of-flight mass spectrometer. All instruments had a standard PM<sub>1</sub> lens and were sampled from the roof without a cyclone.

The AMS and ACSM instruments were calibrated for ionization efficiency of nitrate and relative ionization efficiency of ammonium and sulfate using size-selected single component particles of ammonium nitrate or ammonium sulfate following Budisulistiorini et al.<sup>51</sup> HR-ToF-AMS data were analyzed with Squirrel (1.631) and Pika (1.231) analysis software running on Igor 7 (WaveMetrics, Inc.). ACSM data was analyzed with Tofware (3.2.40211B2) or ACSM Local (v1.6.1.1). The collection efficiency (CE) was set to 0.5 for all data.<sup>52</sup> Positive matrix factorization (PMF), a typical statistical method for analyzing OA contributions to PM, was used to determine source factor contributions from common AMS PMF factors (e.g., HOA, BBOA, LO-OOA, and MO-OOA). PMF analysis of the HR-ToF-AMS data was performed in the PMF Evaluation Tool (PET 3.06).<sup>74</sup> Mass spectra for other sources or urban areas for comparison were from the references herein (Tables S2 and S3).

**2.2. Oxidation Chamber Experiments.** For short-term (i.e., less-aged) experiments, gas-phase emissions were sampled off of a large piece (99.3 g) of recently paved (i.e., collected ~28 h after application) asphalt from an arterial roadway (grade unknown) that was heated to 140 °C with no UV exposure to the sample. The fumes were injected via a Teflon tube into a 10 m<sup>3</sup> Teflon chamber with 1 slpm clean airflow to evaluate the production of primary OA without photo-oxidation. Subsequently, the UV lights (peak λ = 368 nm) were turned on to initiate secondary production under high NO<sub>x</sub> (4.5 ppm) conditions via HONO photolysis. HONO was produced from reacting 25 mL of dilute sodium nitrite solution (10 g/L, >99% Sigma-Aldrich, St. Louis, MO) with sulfuric acid (95/98% Sigma-Aldrich, St. Louis, MO). It was subsequently bubbled into the chamber for photolysis. The chamber was maintained at 25 °C under relatively dry conditions (<10% relative humidity) and an OH concentration of ~1 × 10<sup>-7</sup> molecules cm<sup>-3</sup> during the first hour of oxidation. Deuterated butanol (butanol-*d*<sub>6</sub>; 90% Cambridge Isotope Laboratories) was also injected into the chamber via a heated septum injector as an OH tracer ( $k_{OH} = (3.4 \pm 0.88) \times 10^{-12}$  cm<sup>3</sup> molecule<sup>-1</sup> s<sup>-1</sup>), which was measured using a quadrupole proton transfer reaction mass spectrometer (PTR-MS, Ionicon Analytik, Innsbruck, Austria). The particle-phase effluent from the chamber was measured using an HR-ToF-AMS.

**2.3. Oxidation Flow Reactor Experiments.** Daytime and nighttime oxidative studies of gas-phase asphalt emissions simulating a range of photochemical ages were conducted using a Potential Aerosol Mass OFR (Aerodyne Research, Inc.), which is a horizontal 13 L cylindrical aluminum chamber (46 cm long × 22 cm ID) operated in continuous flow mode with 10 L min<sup>-1</sup> flow through the reactor. The calculated mean residence time in the OFR was approximately 80 s. Across all OFR experiments, the input relative humidity (RH) was controlled with a Nafion membrane and ranged between 30% and 41% at OFR temperatures ranging from 26 to 28 °C. For OH-OFR studies, OH was generated from the combined photolysis of O<sub>2</sub> and H<sub>2</sub>O at λ = 185 nm plus photolysis of O<sub>3</sub> at λ = 254 nm using two low-pressure germicidal mercury lamps. In a subset of experiments, NO<sub>x</sub> was also generated

from O(<sup>1</sup>D) + N<sub>2</sub>O reactions following addition of 260–730 cm<sup>3</sup> min<sup>-1</sup> of N<sub>2</sub>O to the OFR carrier gas flow.<sup>53,54</sup> For NO<sub>3</sub>-OFR studies simulating nighttime chemistry, N<sub>2</sub>O<sub>5</sub> vapor was continuously generated in a laminar flow reactor (LFR) from the reactions NO<sub>2</sub> + O<sub>3</sub> → NO<sub>3</sub> + O<sub>2</sub> and NO<sub>3</sub> + NO<sub>2</sub> → N<sub>2</sub>O<sub>5</sub>. N<sub>2</sub>O<sub>5</sub> was then continuously injected into the dark OFR, where coinjecting asphalt-related emissions were exposed to NO<sub>3</sub> generated from room-temperature thermal decomposition of N<sub>2</sub>O<sub>5</sub>.<sup>55</sup>

Prior to experiments, PG 64-22 grade road asphalt samples were collected from a New Haven, CT paving site and stored in a sealed container. For each experiment, new specimens of this asphalt were heated to surface temperatures achieved during summer daytime in-use and application (60–140 °C) in a custom-made portable heated chamber described in detail elsewhere.<sup>5</sup> The gas-phase emissions were continuously injected into the OFR via a 10 cm heated stainless steel transmission line at a flow rate of 1 L min<sup>-1</sup> with an additional 9 L min<sup>-1</sup> of clean dilution air. The estimated total initial I/SVOC mixing ratios (also including minor contributions of C<sub>10</sub>–C<sub>12</sub> VOCs) introduced to the OFR were 19 ppbv (60 °C) and 112 ppbv (140 °C). To calculate the corresponding total external OH and NO<sub>3</sub> reactivities (OHR<sub>ext</sub>, NO<sub>3</sub>R<sub>ext</sub>) of the emissions, we assumed mean I/SVOC + OH and I/SVOC + NO<sub>3</sub> reaction rate coefficients<sup>56</sup> of 4 × 10<sup>-11</sup> and 1 × 10<sup>-13</sup> cm<sup>3</sup> molecule<sup>-1</sup> s<sup>-1</sup> (applying the acenaphthene-NO<sub>3</sub> rate coefficient<sup>57</sup> of 4.6 × 10<sup>-13</sup> cm<sup>3</sup> molecules<sup>-1</sup> s<sup>-1</sup> to the ~25% aromatic fraction of asphalt I/SVOCs<sup>5</sup> and assuming the remaining I/SVOCs were unreactive toward NO<sub>3</sub>). The calculated OH exposures were approximately (3.0–6.9) × 10<sup>10</sup> molecules cm<sup>-3</sup> s (OHR<sub>ext</sub> = 110 s<sup>-1</sup>) and (1.3–2.6) × 10<sup>11</sup> molecules cm<sup>-3</sup> s (OHR<sub>ext</sub> = 19 s<sup>-1</sup>) using an estimation equation derived by Rowe et al., with an estimated uncertainty of ±50%.<sup>58</sup> These OH exposures correspond to 0.2–0.5 and 1–2 equiv days of atmospheric exposure to [OH] = 1.5 × 10<sup>6</sup> molecules cm<sup>-3</sup> for 140 and 60 °C experiments, respectively.<sup>59</sup> The calculated NO<sub>3</sub> exposures in the OFR were approximately (4–8) × 10<sup>13</sup> molecules cm<sup>-3</sup> s (NO<sub>3</sub>R<sub>ext</sub> = 0.27–0.05 s<sup>-1</sup>) following Lambe et al.<sup>55</sup> These NO<sub>3</sub> exposures correspond to ~1 day of equivalent atmospheric exposure to [NO<sub>3</sub>] = 5.0 × 10<sup>8</sup> molecules cm<sup>-3</sup> s.<sup>57</sup> In all experiments, the particle-phase effluent from the OFR was analyzed using an Aerodyne ToF-AMS, while the gas-phase effluent was measured using a Vocus proton transfer reaction (PTR)-ToF mass spectrometer in a subset of experiments (TOFWERK AG).

### 3. RESULTS AND DISCUSSION

**3.1. Ambient Observations of Asphalt-Related Organic Aerosol.** AMS-based field measurements were performed at the Aerodyne Research site in Billerica, MA in August 2014. These measurements coincided with a number of paving projects in areas surrounding Aerodyne including documented projects on I-95 (MA DOT Project 606170) as well as other paving activities nearby (e.g., US Route 3) (Figure S1). Aerodyne Research is approximately 7 km north/northwest of I-95. During the day, the wind was typically from the south, and the average windspeed was 3–5 km h<sup>-1</sup> meaning that paving emissions would arrive at Aerodyne in about 1–2 h or less in the case of more nearby paving (Figure S2). At night, windspeeds were very low, typically below 0.5 km h<sup>-1</sup> and wind direction was variable. The observations provided the opportunity to investigate the chemical composition of primary and secondary asphalt-related OA

beyond the immediate vicinity of a freshly paved surface. Figure 1 shows a large increase in monthly average PM<sub>1</sub>-sized

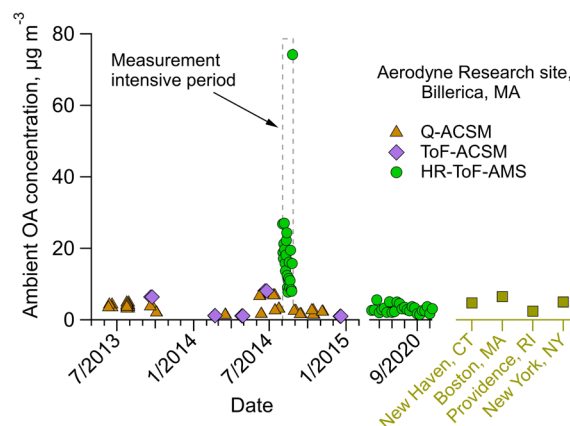


**Figure 1.** Daily averaged ambient OA concentrations at the Aerodyne Research rooftop site in Billerica, MA using 3 variants of aerosol mass spectrometers, with average ambient OA concentrations for nearby urban areas (brown) for comparison, including New Haven (2014),<sup>60,63</sup> Boston (2008),<sup>61</sup> Providence (2022),<sup>60</sup> and New York City (2014).<sup>62,63</sup> The ambient OA concentrations for New Haven and Providence were estimated using the annually averaged measurements of organic carbon via EPA's Chemical Speciation Network<sup>60</sup> using an organic mass-to-organic carbon (OM:OC) ratio of 2 based on prior studies.<sup>64,65</sup> The calculated OA concentrations were consistent with previous airborne measurements of ambient organic aerosol in these regions.<sup>62</sup>

OA concentrations (monthly average: 18 ± 13 µg m<sup>-3</sup>) at the Aerodyne site in August 2014. This enhancement is observed when compared not only to the rest of 2013–2014 (average: 3.3 ± 1.9 µg m<sup>-3</sup>, excluding August) but also to August/September 2020 (monthly average: 3 ± 2 µg m<sup>-3</sup>), the closest year for which we had a late summer month of AMS data sampled from the Aerodyne roof. The 2020 average at Aerodyne is similar to regional OA in 2022 in other urban areas in the northeast US (3.1 ± 0.6 µg m<sup>-3</sup>, Figure 1).<sup>60–62</sup> Figure 2 shows the AMS measurements during August 2014 in more detail. In comparison to before and after the measurement intensive period, the OA concentrations were elevated throughout the month (Figures 1 and 2a). During August 1–11, OA concentrations ranged between 8.5 and 66 µg m<sup>-3</sup> (2 min averages) (Figure 2a) followed by a decrease over next 3 days due to minor precipitation events (i.e., 0.8–17 µg m<sup>-3</sup>). Thereafter, OA was generally elevated again during August 16–25, ranging between 4 and 39 µg m<sup>-3</sup>. The highest loadings were observed on August 26 reaching a 24-h average of 90 ± 79 µg m<sup>-3</sup> with a range of 27–516 µg m<sup>-3</sup> at 2 min resolution. For comparison, OA at the same location averaged 3 ± 2 µg m<sup>-3</sup> during August–September 2020, which was similar to the 2013–14 measurements outside of the paving period.

The persistent OA enhancements in August 2014 suggested prolonged emissions during the nearby road paving project. This was not a region-wide enhancement as regional daily PM<sub>2.5</sub> measured at the MA Department of Environmental Protection von Hillern station (18 miles away) was similar across 2014–2020 (Figure S3b,c). The local OA was enhanced by a factor of 5.1 when normalized to regional PM<sub>2.5</sub> (i.e., ratio of medians in Figure 2a inset), highlighting the proximity of the source. Despite the lingering effects of the pandemic-

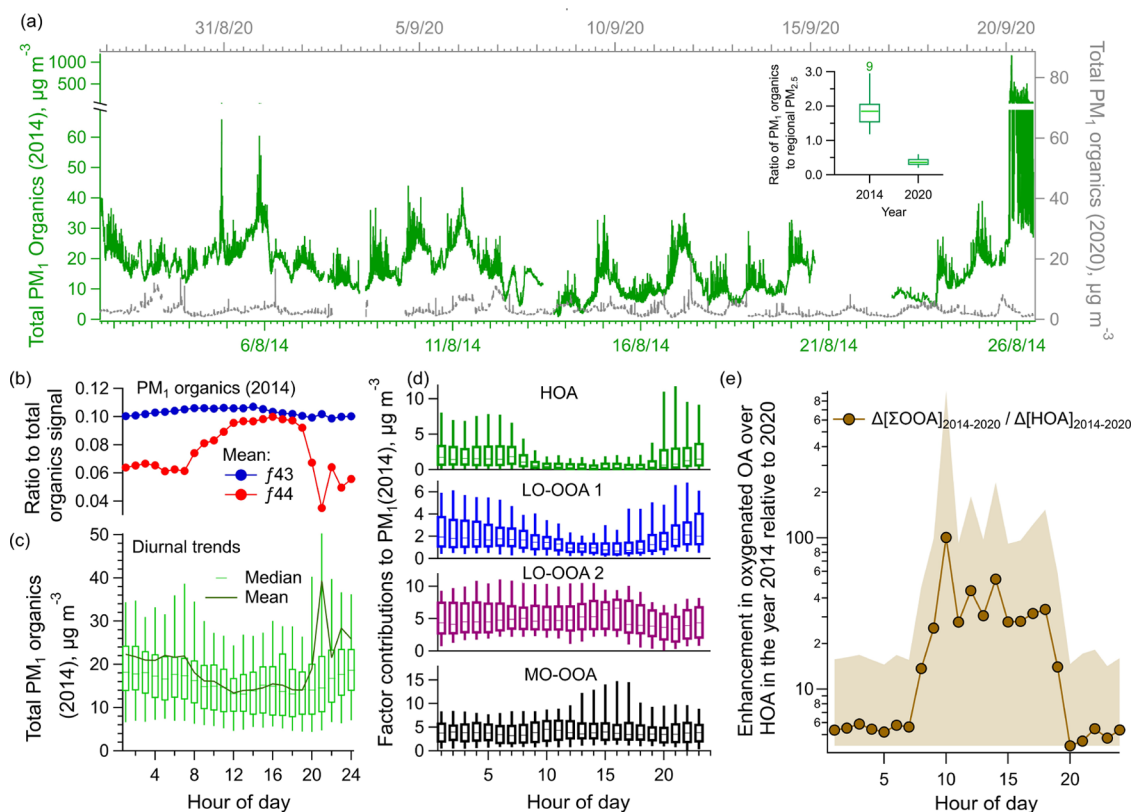


**Figure 2.** (a) OA concentrations ( $\text{PM}_1$ ) measured with an AMS during August 2014 and September 2020 at the Aerodyne Research rooftop site, with (inset) a comparison of local OA to regional  $\text{PM}_{2.5}$  ratios for 2014 and 2020 showing 0th, 25th, 50th, 75th, and 100th percentiles, despite similar regional  $\text{PM}_{2.5}$  concentrations (2014:  $9.2 \mu\text{g m}^{-3}$ ; 2020:  $8.0 \mu\text{g m}^{-3}$ ; Figure S3). Diurnal trends in August 2014 for (b)  $f_{43}$  and  $f_{44}$  ion fragments of the AMS spectra with (c) mean and median concentrations of total measured OA and (d) source factor contributions to OA in August 2014. (e) Diurnal enhancement in total oxygenated organic aerosol over HOA ( $\Sigma\text{OOA}/\text{HOA}$ ) in August 2014 relative to September 2020. All data are in EST.

related shutdown, small changes in traffic volume in 2020 were not enough to explain the large difference in OA in August 2014 relative to that in 2020 (Figure S3a). Furthermore, the size distribution of measured OA was different between the two periods. The ion signal at  $m/z$  57 (characteristic fragment for hydrocarbons) peaked at  $\sim 550$  nm in August 2014, shifted from more typical observations in September 2020 ( $\sim 375$  nm) and with 8 times higher mass loading (Figure S4).

The five OA factors determined via PMF (Section S1, Figures S5–S7) for August 2014 and three for September 2020 (Figures S8 and S9) showed different diurnal trends between the two periods that would arise from variations in contributing sources. For example, HOA in August 2014, during the road paving operations, was typically high overnight, from evening to early morning (8 PM–6 AM) (Figure 2d), as opposed to morning (6 AM–noon) enhancement in September 2020 typical of commute-related maxima due to vehicular emissions (Figures S7–S9). Furthermore, the maximum nighttime HOA averages were 2–6.5 times higher in August 2014 than in September 2020. Daytime HOA was similar across the 2 periods, consistent with major roadway asphalt application activities often occurring at night. Yet, the amount of OOA during daylight hours was significantly enhanced in August 2014 relative to September 2020 (Figures 2b,e and S10), suggesting SOA production leading to average  $\Sigma\text{OOA}/\text{HOA}$  ratios exceeding  $20 \mu\text{g}/\mu\text{g}$ .

More broadly, the mean diurnal OA concentrations in August 2014 showed meteorologically influenced trends

(Figure 2c). The mean concentration dropped from  $22 \mu\text{g m}^{-3}$  at 7 AM to a minima of  $13 \mu\text{g m}^{-3}$  at noon, increasing some throughout the remainder of the day before returning to elevated levels with nightfall (i.e.,  $22$ – $40 \mu\text{g m}^{-3}$ ). The contribution of hydrocarbon-like organic aerosol (HOA) to total OA was significantly reduced between 8 AM and 6 PM, while the three factors contributing to total oxygenated organic aerosol (OOA) showed trends distinct from each other.

The less oxidized OOA factor (LO-OOA1) was characterized by a major  $\text{C}_2\text{H}_3\text{O}^+$  fragment on  $m/z$  43 in addition to  $\text{C}_3\text{H}_7^+$  and an O:C ratio of 0.25. LO-OOA1 was likely affected by boundary layer dilution in the afternoon (Figure 2d: LO-OOA1) with median diurnal concentrations dropping from nighttime averages of  $1.4 \mu\text{g m}^{-3}$  to  $0.6 \mu\text{g m}^{-3}$  in the afternoon. These diurnal patterns varied from LO-OOA2, which remained elevated throughout the day but dropped in the late evening, suggesting differences in OOA formation pathways that may be associated with emissions pathways or chemical processes across the gas and particle phase or possibly variations in direct HOA emissions with the onset of paving activity. LO-OOA2 was more oxidized than LO-OOA1 with a higher O:C ratio of 0.5 and greater  $\text{CO}_2^+$  signal on  $m/z$  44. More oxidized OOA (MO-OOA) was the most aged, with an O:C ratio of 0.8. The median diurnal concentration of MO-OOA was relatively similar across both the night and day, despite enhanced daytime dilution possibly due to enhanced OOA production and aging from atmospheric oxidation of precursor emissions or additional production pathways.

On average, the total OOA including all observed OOA factors was a factor of 8 higher in August 2014 compared to September 2020 (Figures 2, S6, and S8), with average contributions of  $11.5 \pm 5.7 \mu\text{g m}^{-3}$  vs  $1.5 \pm 0.8 \mu\text{g m}^{-3}$ , respectively. For comparison, average HOA contributions were  $1.6 \pm 2.5 \mu\text{g m}^{-3}$  vs  $0.5 \pm 0.4 \mu\text{g m}^{-3}$  during the respective intensive periods.  $\Sigma\text{OOA}/\text{HOA}$  ratios varied dynamically (Figure 2a,e), likely with on-site activities (e.g., application) and environmental conditions (e.g., solar irradiance), ranging from 0.8 to 267.4 (at hourly resolution) with an overall average of  $24.2 \pm 34.0 \mu\text{g} \mu\text{g}^{-1}$  during the 2014 measurement intensive period, corresponding to  $\sim 88\%$  of OA during the paving period occurring as OOA rather than HOA on average. For comparison, when the 2020 average HOA and OOA were subtracted to consider only elevated levels in 2014, this value varied over the course of the day and was  $\sim 90\%$  OOA on average ( $\Delta[\Sigma\text{OOA}]_{2014-2020}/\Delta[\text{HOA}]_{2014-2020} = 9.2 \pm 14.7 \mu\text{g} \mu\text{g}^{-1}$ ) over the 1-month measurement period, similar to previous work, which reported that oxygenated OA formed postapplication can exceed primary OA formed during application by a factor of 9–10.<sup>30</sup>

Overall, ambient observations showed substantially enhanced OA concentrations in August 2014 when road paving occurred nearby, though this project is not assumed to be representative of all projects as the OA contributions from paving activities are expected to vary with asphalt feedstocks (e.g., composition), material properties (e.g., modifier additions), application methods (hot vs warm mix), environmental conditions, and other site specifics (e.g., project size, pavement thickness). The authors are also not aware of the exact asphalt grade or any added modifiers. We also note that, while our analysis suggests a major role of asphalt-paving sources in the elevated ambient OA levels, other contributing sources during the observations in 2014 and 2020 may also exist, and gasoline- and diesel-powered construction equipment used during paving likely also contributed to both HOA- and OOA-precursor emissions in August 2014. However, it was not possible to isolate their impact via the measurements in this study.

**3.2. Laboratory Investigation of Asphalt-Related Organic Aerosol.** Field observations of OA from paving activities emphasized the need for laboratory chamber and OFR experiments for the purpose of comparing the resulting OA spectra to ambient measurements. In these tests, gas-phase precursor emissions from road asphalt at application ( $140 \text{ }^\circ\text{C}$ ) and summertime daytime surface ( $60 \text{ }^\circ\text{C}$ ) temperatures were aged for a few hours and up to 1–2 equiv days simulating urban oxidation conditions (Table S1). The results showed that asphalt-related OA can range from hydrocarbon-like to highly aged organic aerosol depending on differences in asphalt temperature and oxidation conditions. These results are discussed in detail in the following subsections.

**3.2.1. Chamber OA from High-Temperature Paving-Related Emissions.** Short-term daytime aging was simulated in CMU's oxidation chamber to study the chemistry of emissions immediately following high-temperature asphalt application. Gas-phase precursors emitted at  $140 \text{ }^\circ\text{C}$  were injected into a seedless, oxidant-free (hereon: "dark") chamber; then, the lights were turned on after 3 h to initiate photo-oxidation. We observed that injected precursors rapidly formed unaged hydrocarbon-like OA within minutes under dark conditions (Figures 3 and S11). This dark chamber OA ( $\text{HOA}_{\text{DC}}$ ) had mass spectra similar to previous ambient AMS

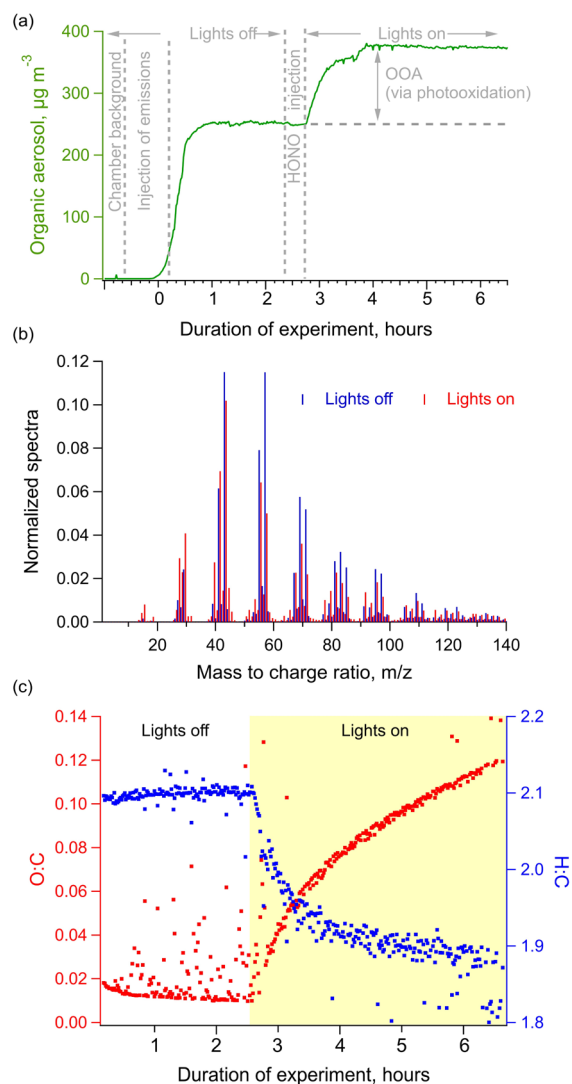


**Figure 3.** Asphalt-related OA formed in short-term chamber experiments from emissions at application temperatures. (a) OA concentrations measured via AMS (diameter  $\leq 1 \mu\text{m}$ ; wall-loss corrected) across the duration of the experiment. (b) AMS spectra of OA produced under dark conditions and following photo-oxidation with chamber lights on. (c) Bulk O:C and H:C ratios for organic aerosol before and during photo-oxidation.

measurements (cosine similarity:  $12\text{--}16^\circ$ ) made directly downwind of road paving,<sup>35</sup> suggesting representative experimental conditions (Figure S12).

The ambient HOA factor observed during August 2014 road paving in Billerica ( $\text{HOA}_{\text{BL14}}$ ) was very similar to the  $\text{HOA}_{\text{DC}}$  from the chamber study (cosine similarity:  $15^\circ$ ). Both  $\text{HOA}_{\text{DC}}$  and  $\text{HOA}_{\text{BL14}}$  were relatively unaged OA with comparable O:C ratios (0.03 vs 0.05) that were much lower than 0.2 in HOA from September 2020 ( $\text{HOA}_{\text{BL20}}$ ). The AMS spectra of  $\text{HOA}_{\text{DC}}$  was dominated by fragments with ion formula  $\text{C}_n\text{H}_{2n+1}^+$  (e.g.,  $m/z$  29, 43, 57, and 71) that represented acyclic alkanes. Other major fragments included  $\text{C}_n\text{H}_{2n-1}^+$  (e.g.,  $m/z$  27, 41, 55, 69, and 83) and  $\text{C}_n\text{H}_{2n-3}^+$  (e.g.,  $m/z$  67, 79, 81, 95, and 109) that are both typically cycloalkanes<sup>66</sup> and aromatic fragments (e.g.,  $m/z$  77, 91, 105, and 119). The dominance of nonaromatic fragments was consistent with the previously reported composition of asphalt-related precursor emissions at  $140 \text{ }^\circ\text{C}$ ,<sup>5</sup> and the aromatic fraction would also be

somewhat susceptible to ring-opening during oxidation.<sup>67,68</sup> The contributions from functionalized fragments ( $C_xH_yO_1$ ) to the HOA<sub>DC</sub> spectra were expectedly minor under dark chamber conditions and were likely primary emissions (Figure S11).

After 2.4 h, HONO was injected into the chamber, and UV lights were turned on to simulate daytime conditions. This led to a 50% increase in OA concentrations after the equivalent of 6 h of atmospheric aging, indicating SOA formation during which the bulk O:C ratio increased from 0.03 to 0.1 and the H:C decreased from 2.1 to 1.9 (Figure 3c). Via a modeling analysis, a similar change in ambient asphalt-related OA concentration was attributed to photochemistry by Seltzer et al.<sup>14</sup> By comparison, the enhancement in the year 2014 relative to 2020 ( $\Delta\Sigma\text{OOA}/\Delta\text{HOA}$ ) averaging  $9.2 \pm 14.7 \mu\text{g } \mu\text{g}^{-1}$  in ambient observations (Figure 2e) with greater overall O:C ratios indicates that, over longer time scales following application, the majority of asphalt-related OA production will exhibit itself as oxygenated SOA, with variations with time of day, season, source proximity, and degree of photochemical aging. While Figure 3a has been corrected for particle losses to the chamber walls, the SOA production in this photooxidation experiment is a lower bound due to well-known losses of reactive I/SVOCs<sup>69,70</sup> to the walls of the reaction chamber during the 2.5 h dark period.

The photo-oxidized chamber OA (OA<sub>LC</sub>) showed comparable mass spectra to ambient LO-OOA1 from August 2014 (cosine similarity: 17°) with a similar H:C ratio (OA<sub>LC</sub>: 1.9; LO-OOA1: 1.8). Yet, OA<sub>LC</sub> was slightly less oxygenated than the ambient LO-OOA1 (O:C, 0.1 vs 0.25) with oxygenated fragments constituting 21% of OA<sub>LC</sub> (Figure S13) and ~35% of LO-OOA1. This broadly suggested that LO-OOA1 observed in the ambient measurements was inclusive of a combination of less-aged gas- or particle-phase asphalt-related emissions following paving, though some contributions from other combustion-based sources (e.g., diesel vehicles) is also possible.

Photochemical aging also introduced differences between the HOA<sub>DC</sub> and OA<sub>LC</sub> spectra. OA<sub>LC</sub> constituted more cyclic species ( $f_{55}:f_{57} = 1.3$ ) than HOA<sub>DC</sub> (0.7), which may be the result of the oxidation and partitioning of gas-phase organic precursors and/or the aging of particle-phase species. The spectra of both OA types had similar relative contributions from large (>150  $m/z$ ) and smaller hydrocarbon fragments (e.g.,  $m/z$  41, 43, 55), but OA<sub>LC</sub> expectedly had more oxygenated fragments (e.g.,  $m/z$  28, 31, 44–46, 51), which is reflective of contributions from both unaged or less-aged hydrocarbons and condensed secondary oxygenated species.

**3.2.2. OA from Longer-Term Simulated Aging Experiments.** Gas-phase precursors emitted at both 140 and 60 °C were aged for longer effective durations (0.2–2 equiv days) in an OFR. The extent of aging varied across experiments depending on the type of emissions and reactor conditions. The OA produced from emissions at 140 °C in unseeded tests (OFR-OA<sub>US140</sub>) was less aged (0.2–0.5 equiv day) and resembled HOA. The mass spectrum of OFR-OA<sub>US140</sub> was dominated by hydrocarbon fragments with an O:C ratio of 0.05, comparable to 0.03 for HOA<sub>DC</sub>. Yet, 12% of  $f_{43}$  in its mass spectra was constituted by  $C_2H_3O^+$ , which was entirely  $C_3H_7^+$  in HOA<sub>DC</sub>. Moderately aged OA from a seeded experiment with the same emissions (OFR-OA<sub>S140</sub>) had an O:C ratio of 0.18, yet hydrocarbon fragments still dominated the mass spectrum.

We also found that daytime (OH) vs nighttime (NO<sub>3</sub>) unseeded oxidation of emissions at 140 °C produced OA with comparable mass spectra (Figure S14) and bulk properties (H:C, 1.8; O:C, 0.05 vs 0.09). This was somewhat unexpected because NO<sub>3</sub> is a more selective oxidant and is expected to react primarily with PAHs and other unsaturated compounds. PAHs constituted <10% of the total precursor mass, and the prevalence of functionalized organics was less than hydrocarbons by an order of magnitude.<sup>5</sup> Yet, only a slight difference was observed in the chemical composition of OA. This could be due to nucleation of unoxidized precursors being the dominant pathway of particle formation from emissions at 140 °C, as observed with HOA<sub>DC</sub> in chamber tests. Despite similar chemical properties, the peak OA production of  $0.8 \pm 0.4 \text{ mg OA min}^{-1} \text{ kg}^{-1}$  asphalt observed under NO<sub>3</sub> oxidation was slightly lower than  $2.5 \pm 0.2 \text{ mg SOA min}^{-1} \text{ kg}^{-1}$  asphalt from unseeded daytime oxidation tests as well as  $4 \pm 2.3 \text{ mg OA min}^{-1} \text{ kg}^{-1}$  asphalt estimated in previous work.<sup>5</sup>

While the gas-phase emissions at 140 °C readily formed OA independent of photochemistry, precursor emissions at 60 °C primarily included IVOCs<sup>5</sup> that produced SOA mainly after undergoing photo-oxidation. Under daytime unseeded oxidation conditions, the resulting OA (OFR-OA<sub>US60</sub>) was highly aged with an O:C ratio of 0.7 and primarily constituted oxygenated compounds (62%  $C_xH_yO_1$  and  $C_xH_yO_{>1}$  species). For reduced emissions at lower temperatures (e.g., 40–50 °C), the  $f_{44}$  fraction in OA further increased by 35–80%, indicating further photooxidation for aerosol formation with reduced OHR<sub>ext</sub> (Figure S15). We also observed that gas-phase oxidation products measured with PTR-ToF mainly constituted small compounds with less than 8 carbon atoms in oxidation experiments with emissions at 140 °C. However, the fraction of larger gaseous oxidation products (i.e.,  $C_{\#} > 8$ ) increased considerably in tests at 60 °C, though their absolute abundance was greater at 140 °C. This was possibly due to relatively lower OA mass loading in the reactor at 60 °C, which reduced the condensational sink and gas-to-particle partitioning of gas-phase species as well as the OHR<sub>ext</sub>, thus increasing the OH exposure of injected precursors (aged 1–2 equiv days) (Figure S16).

In addition to oxidized species, we also note minor contributions from precursor sulfur containing organic compounds that were observed in the particle phase as sulfate (HRSO<sub>4</sub>). Their signal enhanced linearly with total organics (HROrg) and was sensitive to UV exposure in OFR tests (Section S2, Figure S17). Consistent with laboratory observations, a significant enhancement in sulfate was also observed in Billerica during road paving in 2014 but not in 2020 (Figure S18), suggesting that high-temperature road paving could also make minor contributions to ambient organosulfates at paving temperatures (Figures S17–S18), but their absolute impact may depend on the asphalt material used in paving operations.

The chamber and OFR tests showed that gas-phase emissions from asphalt can form OA in the atmosphere via both direct condensation and secondary oxidation pathways. Both of these pathways were likely associated with enhancements in ambient OA downwind in Billerica during paving in 2014, yet asphalt-related OA can span a range of aging and chemical composition dependent on the type of emissions and oxidation conditions. While high-temperature (140 °C) applications show a greater degree of HOA-like or less-aged aerosols, the OA formed via photo-oxidation spans slightly-

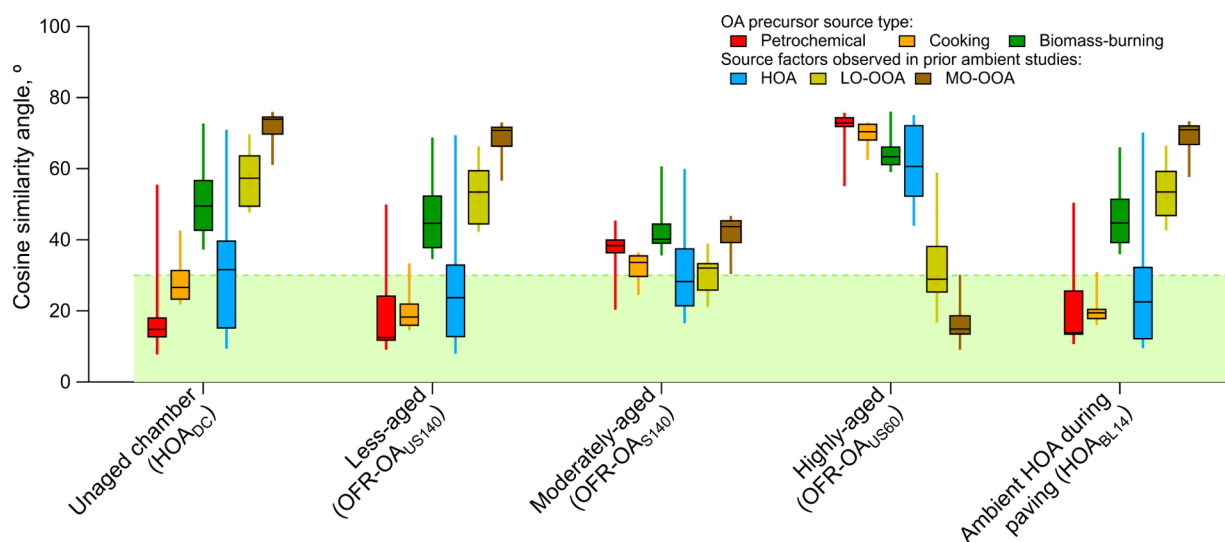


**Figure 4.** Comparison of OA produced from asphalt-related chamber and OFR experiments, as well as the HOA factor measured at the Aerodyne site during the road-paving event, with OA obtained from petrochemical, cooking, and biomass burning emissions in prior laboratory experiments (see Table S2 for study descriptions) and with HOA, LO-OOA, and MO-OOA factors from previous ambient studies (Table S3). The box plots show 0th, 25th, 50th, 75th, and 100th percentiles in cosine similarities, and the green shaded region represents a cosine angle of  $\leq 30^\circ$  within which the spectra are considered comparable. Note: All experiments except the highly aged (OFR) were performed with precursor emissions at paving temperature ( $140^\circ\text{C}$ ), while the highly aged (OFR) involved precursor emissions at summertime road surface temperatures ( $60^\circ\text{C}$ ). The terms less-, moderate-, and highly aged depend upon the degree of oxidation of the OA formed in the OFR and are not to be confused with the equivalent aging during an experiment.

highly-aged OA under different emission and oxidation conditions.

**3.3. Comparison of Asphalt-Related OA with Source-Specific and Typical Urban Factors.** Here, we examine similarities in the chemical composition of asphalt-related OA from our experiments and ambient data with OA from other sources and ambient factors previously observed via PMF analysis. PMF often groups OA from sources that have similar chemical features. So, asphalt-related OA from our mix of laboratory and ambient measurements was compared to other urban sources and ambient factors to evaluate how its contributions might appear in comparison to different sources or urban areas in prior studies.

**3.3.1. Comparisons to Source-Specific OA from Previous Experiments.** First, we compare OA from our asphalt tests with prior laboratory or near-source observations of OA from a broad range of sources, including fresh OA resulting from petrochemical, cooking, wood-burning, and biomass-burning emissions. Asphalt-related OA could be difficult to isotopically differentiate from traditional combustion-based sources (e.g., vehicular exhaust) that are also derived from petroleum feedstocks.<sup>71–73</sup> However, its mass spectral features may vary, depending on precursor and aging conditions. We obtained unit mass resolution spectra of these sources from the AMS spectral database (Table S2)<sup>74,75</sup> and compared them over a mass range of  $m/z$  12–125, which constituted 90–95% of the total ion signal for different OA included in this analysis. The spectra of multiple sources within each category (e.g., different types of biomass-burning OA) were averaged prior to a category-wide comparison and are reported in Table S2. Lastly, each spectrum was normalized by the total ion signal in this range and compared via linear correlation and cosine angle similarity.

In these comparisons, we primarily discuss asphalt-related OA at hot-mix paving temperature ( $140^\circ\text{C}$ ) because, at lower temperatures ( $60^\circ\text{C}$ ) after several days of photochemical

aging, OFR-OA<sub>US60</sub> was highly aged with  $f_{44}$  and  $f_{28}$  constituting >40% of the mass spectra and expectedly did not correlate with any of the experiments without extensive oxidation in this study. On the other hand, asphalt OA at  $140^\circ\text{C}$  was comparable to OA from petrochemical sources (Figures 4 and S19). For example, our chamber (HOA<sub>DC</sub>, OA<sub>LC</sub>) and unseeded OFR (OFR-OA<sub>US140</sub>) tests formed OA similar to combustion emissions from gasoline, diesel, and plastics (cosine angle:  $8\text{--}24^\circ$ ; linear correlation coefficient,  $r > 0.85$ ) with comparable  $m/z$  44:43 and 55:57 ratios (Figures S19 and S20). Among all cases, the strongest similarities were observed between HOA<sub>DC</sub> and OA from gasoline emissions and lubricating oil ( $8^\circ$ ,  $r > 0.95$ ) (Figure S21). HOA<sub>DC</sub> was also highly comparable to average OA from different diesel exhaust studies ( $r > 0.9$ ,  $18^\circ$ ). Yet, it differed from diesel generator exhaust ( $r < 0.8$  and  $36^\circ$ ), which was more similar to aged OA<sub>LC</sub> and OFR-OA<sub>S140</sub> ( $r > 0.9$  and  $21^\circ$ ). Outside gasoline and diesel sources, flaming coal-based OA showed comparable spectral features ( $12\text{--}34^\circ$ ) and similar  $m/z$  44:43 and levoglucosan  $m/z$  ( $f_{60}$ ) values. Asphalt-related OA was also sometimes similar to OA from meat-cooking emissions ( $16\text{--}35^\circ$ ;  $r > 0.85$ ) with comparable  $m/z$  44:43 ratios (Figure S15), yet with  $m/z$  55:57 and  $f_{60}$  values lower by factors of 2 and 10, respectively.

In contrast, asphalt OA was distinct from most wood/biomass burning-related OA (WBOA/BBOA) in our comparisons where mass spectra exhibited weak ( $r < 0.75$ ) linear correlations and large cosine angles ( $36\text{--}49^\circ$ ) (Figures 4 and S19). WBOA and BBOA showed strong levoglucosan signals ( $f_{60}$ ), which were absent in asphalt OA. It was also more oxygenated with an  $m/z$  44:43 ratio of 0.25–1.4 versus 0.04–0.15 for asphalt and other petrochemical sources (Figures S15 and S20).

**3.3.2. Comparisons to Source Apportioned OA Factors from Other Ambient Urban Areas.** The unaged asphalt-related OA from our laboratory tests at application temper-

atures resembled prior urban HOA factors from AMS measurements in megacities in the U.S., Europe, and China (Figures 4 and S22, Table S3)<sup>75</sup> as well as the ambient HOA factor observed in Billerica during paving in 2014 (Figure S23), which is consistent with prior observations by Faber et al.<sup>35</sup> who examined paving-adjacent enhancements closely resembling HOA (Figure S12). The application-related OA after 2.5 h of aging in our chamber tests (OA<sub>LC</sub>, Figure 3) was also comparable to ambient HOA factors from prior studies (cosine:  $24^\circ \pm 14^\circ$ ) (Table S3, Figure S24) with expected variations in cosine similarity likely arising from slightly oxygenated aerosol mass fragments influencing ambient HOA factors. Interestingly, the unaged HOA from the chamber (HOA<sub>DC</sub>) was broadly comparable (i.e., cosine  $<30^\circ$ ) to HOA from 40% of included ambient sites, with this fraction increasing to 80% for the slightly aged OA<sub>LC</sub>. Similarly, OA from both seeded and unseeded OFR experiments (OFR-OA<sub>S140</sub>, OFR-OA<sub>US140</sub>) resembled HOA from nearly 50% of the cities in the prior work (Table S3). Yet, this similarity to urban HOA factors (and other OOA factors below) does not suggest that the majority of HOA (or OOA) in urban areas is asphalt-derived but demonstrates the difficulty in distinguishing asphalt-related OA from other petroleum-related sources. In the case of HOA, this is a reflection of asphalt's petroleum feedstocks and the inherent nature of PMF source factors representing a mix of sources with similar molecular signatures.

Expectedly, increased aging reduced similarity to ambient HOA factors but moderately and highly aged OFR-OA also showed greater similarities to LO-OOA and MO-OOA ambient factors observed in both the 2014 near-paving ambient measurements and other urban studies (Figure S22). For example, in Figure 4, the highly oxidized OFR-OA<sub>US60</sub> was expectedly dissimilar to HOA from all sites (cosine similarity  $> 30^\circ$ ) but was very similar to MO-OOA obtained from all prior ambient studies considered here (Table S3).

In summary, these comparisons with various major sources and ambient urban OA PMF source factors show that distinguishing asphalt-related OA from the range of urban sources of direct OA and reactive precursors is challenging. While fresh OA from hot-mix asphalt paving was different from biomass-burning and meat cooking, it was statistically similar to OA from gasoline- and diesel-related sources (Figures 4 and S23) as well as HOA source factors in urban studies. Furthermore, atmospheric aging of primary condensed OA or SOA formed from gas-phase precursors would contribute to the typically observed LO-OOA and MO-OOA factors, like those seen in the 2014 ambient measurements. In the case of highly aged OA from asphalt-related emissions at summertime pavement temperatures, like the 60 °C OFR studies here, the resulting MO-OOA would be largely indistinguishable under ambient conditions (Figure 4). These similarities across multiple atmospheric ages, coupled with the fossil isotopic signature of asphalt-related emissions,<sup>11</sup> could potentially result in misattribution of asphalt-related OA to other prominent urban sources in ambient measurements and top-down assessments of emissions across asphalt's lifecycle. Further research is warranted to develop methods (e.g., identification of marker species, isolating volatility-dependent contributions) to constrain the impact of asphalt-related emissions on urban OA.

## ■ ASSOCIATED CONTENT

### SI Supporting Information

The Supporting Information is available free of charge at <https://pubs.acs.org/doi/10.1021/acsestair.4c00193>.

Overview of the Billerica sampling site location and wind data; supplemental ambient observations, positive matrix factorization results, and their interpretation; additional details on laboratory oxidation experiments and associated results; supplemental comparisons with organic aerosol mass spectra from previous ambient and chamber experiments (PDF)

## ■ AUTHOR INFORMATION

### Corresponding Author

Drew R. Gentner – Department of Chemical and Environmental Engineering and School of the Environment, Yale University, New Haven, Connecticut 06511, United States; Email: [drew.gentner@yale.edu](mailto:drew.gentner@yale.edu)

### Authors

Peeyush Khare – Department of Chemical and Environmental Engineering, Yale University, New Haven, Connecticut 06511, United States; Laboratory of Atmospheric Chemistry, Paul Scherrer Institute, 5232 Villigen, Switzerland; Present Address: Institute of Climate and Energy Systems, ICE-3: Troposphere, Forschungszentrum Jülich GmbH, 52428 Jülich, Germany; [orcid.org/0009-0001-1039-8759](https://orcid.org/0009-0001-1039-8759)

Jo Machesky – Department of Chemical and Environmental Engineering, Yale University, New Haven, Connecticut 06511, United States; Present Address: United States Environmental Protection Agency, Durham, North Carolina 27709, United States.

Leah Williams – Aerodyne Research Inc., Billerica, Massachusetts 01821, United States; [orcid.org/0000-0002-8505-9591](https://orcid.org/0000-0002-8505-9591)

Mackenzie Humes – Center for Atmospheric Particle Studies, Carnegie Mellon University, Pittsburgh, Pennsylvania 15213, United States; Present Address: California Air Resources Board, Riverside, California 92507, United States.; [orcid.org/0000-0003-3726-191X](https://orcid.org/0000-0003-3726-191X)

Edward C. Fortner – Aerodyne Research Inc., Billerica, Massachusetts 01821, United States

Manjula Canagaratna – Aerodyne Research Inc., Billerica, Massachusetts 01821, United States

Jordan E. Krechmer – Aerodyne Research Inc., Billerica, Massachusetts 01821, United States; Present Address: Osmo Labs PBC., Somerville, Massachusetts 02144, United States.; [orcid.org/0000-0003-3642-0659](https://orcid.org/0000-0003-3642-0659)

Andrew T. Lambe – Aerodyne Research Inc., Billerica, Massachusetts 01821, United States; [orcid.org/0000-0003-3031-701X](https://orcid.org/0000-0003-3031-701X)

Albert A. Presto – Center for Atmospheric Particle Studies, Carnegie Mellon University, Pittsburgh, Pennsylvania 15213, United States; [orcid.org/0000-0002-9156-1094](https://orcid.org/0000-0002-9156-1094)

Complete contact information is available at: <https://pubs.acs.org/doi/10.1021/acsestair.4c00193>

### Notes

The authors declare no competing financial interest.

## ACKNOWLEDGMENTS

We acknowledge funding from U.S. NSF (grants: AGS-2131368 (Aerodyne); CBET-2011362, AGS-2131084 (Yale University); and CBET-1907446, AGS-1848324 (Carnegie Mellon University)). The 2014 ambient data in Billerica, MA was collected with support from the U.S. Department of Energy (DESC0004698). We also acknowledge the U.S. EPA; this publication was developed under Assistance Agreement Nos. RD835871 and 83587301 awarded by the U.S. Environmental Protection Agency to Yale University and Carnegie Mellon University, respectively. It has not been formally reviewed by EPA. The views expressed in this document are solely those of the authors and do not necessarily reflect those of the Agency. EPA does not endorse any products or commercial services mentioned in this publication. We also thank Yale Facilities for helping acquire the PG 64-22 road asphalt during a road resurfacing event in New Haven, CT; and Rishabh Shah (formerly at CIRES) for helpful discussions on ToF-AMS analysis.

## REFERENCES

- (1) Hass-Mitchell, T.; et al. Increasing Contributions of Temperature-Dependent Oxygenated Organic Aerosol to Summertime Particulate Matter in New York City. *ACS ES&T Air* **2024**, *1*, 113–128.
- (2) Jimenez, J. L.; et al. Evolution of organic aerosol in the atmosphere. *Science* **2009**, *326*, 1525–1529.
- (3) Kroll, J. H.; Seinfeld, J. H. Chemistry of secondary organic aerosol: Formation and evolution of low-volatility organics in the atmosphere. *Atmos. Environ.* **2008**, *42*, 3593–3624.
- (4) Zhao, Y.; et al. Reducing secondary organic aerosol formation from gasoline vehicle exhaust. *Proc. Natl. Acad. Sci. U. S. A.* **2017**, *114*, 6984–6989.
- (5) Khare, P.; et al. Asphalt-related emissions are a major missing nontraditional source of secondary organic aerosol precursors. *Sci. Adv.* **2020**, *6*, No. eabb9785.
- (6) Gentner, D. R.; et al. Emissions of terpenoids, benzenoids, and other biogenic gas-phase organic compounds from agricultural crops and their potential implications for air quality. *Atmos. Chem. Phys. Discuss.* **2014**, *14*, 5393–5413.
- (7) He, M.; et al. Total organic carbon measurements reveal major gaps in petrochemical emissions reporting. *Science* **2024**, *383*, 426–432.
- (8) Pennington, E. A.; et al. Modeling secondary organic aerosol formation from volatile chemical products. *Atmos. Chem. Phys.* **2021**, *21*, 18247–18261.
- (9) Kroll, J. H.; Seinfeld, J. H. Chemistry of secondary organic aerosol: Formation and evolution of low-volatility organics in the atmosphere. *Atmos. Environ.* **2008**, *42*, 3593–3624.
- (10) Guenther, A. Biological and Chemical Diversity of Biogenic Volatile Organic Emissions into the Atmosphere. *ISRN Atmos. Sci.* **2013**, *2013*, 1–27.
- (11) Khare, P.; Gentner, D. R. Considering the future of anthropogenic gas-phase organic compound emissions and the increasing influence of non-combustion sources on urban air quality. *Atmos. Chem. Phys.* **2018**, *18*, 5391–5413.
- (12) McDonald, B. C.; et al. Volatile chemical products emerging as largest petrochemical source of urban organic emissions. *Science (80-)* **2018**, *359*, 760–764.
- (13) Gkatzelis, G. I.; et al. Observations Confirm that Volatile Chemical Products Are a Major Source of Petrochemical Emissions in U.S. Cities. *Environ. Sci. Technol.* **2021**, *55*, 4332–4343.
- (14) Seltzer, K. M.; et al. Anthropogenic secondary organic aerosol and ozone production from asphalt-related emissions. *Environ. Sci. Atmos.* **2023**, *3*, 1221–1230.
- (15) Wang, F.; et al. Characteristics of VOCs generated during production and construction of an asphalt pavement. *Transp. Res. Part D Transp. Environ.* **2020**, *87*, 102517.
- (16) Cui, P.; Wu, S.; Xiao, Y.; Zhang, H. Study on the deteriorations of bituminous binder resulted from volatile organic compounds emissions. *Constr. Build. Mater.* **2014**, *68*, 644–649.
- (17) Movilla-Quesada, D.; et al. Analysis of Greenhouse Gas Emissions and the Environmental Impact of the Production of Asphalt Mixes Modified with Recycled Materials. *Sustain.* **2021**, *13*, 8081.
- (18) Farshidi, F.; et al. Direct Measurements of Volatile and Semivolatile Organic Compounds from Hot- and Warm-Mix Asphalt. *Transp. Res. Rec.* **2011**, *2207*, 1–10.
- (19) Kriech, D. M.; Crawford, A. C.; Smith, L. A.; Osborn, L. V.; Kriech, A. J. Characterizing asphalt emissions under in-service conditions. *Atmos. Environ. X* **2022**, *16*, 100196.
- (20) Boczkaj, G.; Przyjazny, A.; Kaminski, M. Characteristics of volatile organic compounds emission profiles from hot road bitumens. *Chemosphere* **2014**, *107*, 23–30.
- (21) Kitto, A. M.; et al. Emissions of Volatile and Semi-Volatile Organic Compounds and Particulate Matter from Hot Asphalts. *Environ. Technol.* **1997**, *18*, 121–138.
- (22) Mo, S.; Wang, Y.; Xiong, F.; Ai, C. Effects of asphalt source and mixing temperature on the generated asphalt fumes. *J. Hazard. Mater.* **2019**, *371*, 342–351.
- (23) Jullien, A.; et al. Airborne Emissions Assessment of Hot Asphalt Mixing. *Road Mater. Pavement Des.* **2010**, *11*, 149–169.
- (24) Martin, H.; Kerstin, Z.; Joachim, M. Reduced emissions of warm mix asphalt during construction. *Road Mater. Pavement Des.* **2019**, *20*, S568–S577.
- (25) Gundla, A.; Shane Underwood, B. Molecular weight distribution of asphalt binders from Laser Desorption Mass Spectroscopy (LDMS) technique and its relationship to linear viscoelastic relaxation spectra. *Fuel* **2020**, *262*, 116444.
- (26) Niles, S. F.; Chacón-Patiño, M. L.; Putnam, S. P.; Rodgers, R. P.; Marshall, A. G. Characterization of an Asphalt Binder and Photoproducts by Fourier Transform Ion Cyclotron Resonance Mass Spectrometry Reveals Abundant Water-Soluble Hydrocarbons. *Environ. Sci. Technol.* **2020**, *54*, 8830–8836.
- (27) Tyler, S. C.; Lowe, D. C.; Dlugokencky, E.; Zimmerman, P. R.; Cicerone, R. J. Methane and carbon monoxide emissions from asphalt pavement: Measurements and estimates of their importance to global budgets. *J. Geophys. Res.* **1990**, *95*, 14007.
- (28) Lasne, J.; et al. NO<sub>x</sub> emissions by real-world fresh and old asphalt mixtures: Impact of temperature, relative humidity, and UV-irradiation. *Urban Clim.* **2023**, *49*, 101457.
- (29) Lasne, J.; et al. VOC emissions by fresh and old asphalt pavements at service temperatures: impacts on urban air quality. *Environ. Sci. Atmos.* **2023**, *3*, 1601–1619.
- (30) Humes, M. B.; et al. Primary and Secondary Organic Aerosol Formation from Asphalt Pavements. *Environ. Sci. Technol.* **2023**, *57*, 20034–20042.
- (31) Glatte, T. J.; Chacon-Patino, M. L.; Marshall, A. G.; Rodgers, R. P. Maltene and Asphaltene Contributions to the Formation of Water-Soluble Emerging Contaminants from Photooxidation of Paving Materials. *Energy Fuels* **2022**, *36*, 13060–13072.
- (32) Chong, D.; Wang, Y.; Zhao, K.; Wang, D.; Oeser, M. Asphalt Fume Exposures by Pavement Construction Workers: Current Status and Project Cases. *J. Constr. Eng. Manag.* **2018**, *144*, No. 05018002.
- (33) Xu, Y.; Lindh, C. H.; Jönsson, B. A. G.; Broberg, K.; Albin, M. Occupational exposure to asphalt mixture during road paving is related to increased mitochondria DNA copy number: A cross-sectional study. *Environ. Heal. A Glob. Access Sci. Source* **2018**, *17*, 29.
- (34) McClean, M. D.; et al. Inhalation and Dermal Exposure among Asphalt Paving Workers. *Ann. Occup. Hyg.* **2004**, *48*, 663–671.
- (35) Faber, P.; Drewnick, F.; Borrmann, S. Aerosol particle and trace gas emissions from earthworks, road construction, and asphalt paving in Germany: Emission factors and influence on local air quality. *Atmos. Environ.* **2015**, *122*, 662–671.

- (36) Zhang, X.; et al. Highly Oxygenated Multifunctional Compounds in  $\alpha$ -Pinene Secondary Organic Aerosol. *Environ. Sci. Technol.* **2017**, *51*, 5932–5940.
- (37) Zhang, Y.; et al. Effect of the Aerosol-Phase State on Secondary Organic Aerosol Formation from the Reactive Uptake of Isoprene-Derived Epoxydiols (IEPOX). *Environ. Sci. Technol. Lett.* **2018**, *5*, 167–174.
- (38) Nah, T.; Sanchez, J.; Boyd, C. M.; Ng, N. L. Photochemical Aging of  $\alpha$ -pinene and  $\beta$ -pinene Secondary Organic Aerosol formed from Nitrate Radical Oxidation. *Environ. Sci. Technol.* **2016**, *50*, 222–231.
- (39) Lambe, A. T.; et al. Relationship between oxidation level and optical properties of secondary organic aerosol. *Environ. Sci. Technol.* **2013**, *47*, 6349–6357.
- (40) Chowdhury, P. H.; et al. Exposure of Lung Epithelial Cells to Photochemically Aged Secondary Organic Aerosol Shows Increased Toxic Effects. *Environ. Sci. Technol. Lett.* **2018**, *5*, 424–430.
- (41) Chowdhury, P. H.; et al. Connecting the Oxidative Potential of Secondary Organic Aerosols with Reactive Oxygen Species in Exposed Lung Cells. *Environ. Sci. Technol.* **2019**, *53*, 13949–13958.
- (42) Li, R.; et al. Laboratory studies on secondary organic aerosol formation from crude oil vapors. *Environ. Sci. Technol.* **2013**, *47*, 12566–12574.
- (43) Bahreini, R.; et al. Mass spectral analysis of organic aerosol formed downwind of the deepwater horizon oil spill: Field studies and laboratory confirmations. *Environ. Sci. Technol.* **2012**, *46*, 8025–8034.
- (44) Shah, R. U.; et al. Urban Oxidation Flow Reactor Measurements Reveal Significant Secondary Organic Aerosol Contributions from Volatile Emissions of Emerging Importance. *Environ. Sci. Technol.* **2020**, *54*, 714–725.
- (45) Palm, B. B.; et al. Secondary organic aerosol formation from ambient air in an oxidation flow reactor in central Amazonia. *Atmos. Chem. Phys.* **2018**, *18*, 467–493.
- (46) Kang, E.; et al. Photochemical aging of aerosol particles in different air masses arriving at Baengnyeong Island. *Korea. Atmos. Chem. Phys.* **2018**, *18*, 6661–6677.
- (47) Ahlberg, E.; et al. No Particle Mass Enhancement from Induced Atmospheric Ageing at a Rural Site in Northern Europe. *Atmosphere (Basel)*. **2019**, *10*, 408.
- (48) Janecek, N. J.; et al. Physical properties of secondary photochemical aerosol from OH oxidation of a cyclic siloxane. *Atmos. Chem. Phys.* **2019**, *19*, 1649–1664.
- (49) Liu, P. S. K.; et al. Transmission Efficiency of an Aerodynamic Focusing Lens System: Comparison of Model Calculations and Laboratory Measurements for the Aerodyne Aerosol Mass Spectrometer. *Aerosol Sci. Technol.* **2007**, *41*, 721–733.
- (50) DeCarlo, P. F.; et al. Field-deployable, high-resolution, time-of-flight aerosol mass spectrometer. *Anal. Chem.* **2006**, *78*, 8281–8289.
- (51) Budisulistiorini, S. H.; et al. Intercomparison of an Aerosol Chemical Speciation Monitor (ACSM) with ambient fine aerosol measurements in downtown Atlanta. *Georgia. Atmos. Meas. Technol.* **2014**, *7*, 1929–1941.
- (52) Middlebrook, A. M.; Bahreini, R.; Jimenez, J. L.; Canagaratna, M. R. Evaluation of Composition-Dependent Collection Efficiencies for the Aerodyne Aerosol Mass Spectrometer using Field Data. *Aerosol Sci. Technol.* **2012**, *46*, 258–271.
- (53) Lambe, A.; et al. Controlled nitric oxide production via O(1D)+N<sub>2</sub>O reactions for use in oxidation flow reactor studies. *Atmos. Meas. Technol. Discuss.* **2017**, *10*, 2283–2298.
- (54) Peng, Z.; et al. Model Evaluation of New Techniques for Maintaining High-NO Conditions in Oxidation Flow Reactors for the Study of OH-Initiated Atmospheric Chemistry. *ACS Earth Sp. Chem.* **2018**, *2*, 72–86.
- (55) Lambe, A. T.; et al. Nitrate radical generation via continuous generation of dinitrogen pentoxide in a laminar flow reactor coupled to an oxidation flow reactor. *Atmos. Meas. Technol.* **2020**, *13*, 2397–2411.
- (56) Robinson, A. L.; et al. Rethinking organic aerosol: Semivolatile emissions and photochemical aging. *Science* **2007**, *315*, 1259–1262.
- (57) Atkinson, R. Kinetics and Mechanisms of the Gas-Phase Reactions of the NO<sub>3</sub> Radical with Organic Compounds. *J. Phys. Chem. Ref. Data* **1991**, *20*, 459–507.
- (58) Rowe, J. P.; Lambe, A. T.; Brune, W. H. Technical Note: Effect of varying the  $\lambda = 185$  and 254nm photon flux ratio on radical generation in oxidation flow reactors. *Atmos. Chem. Phys.* **2020**, *20*, 13417–13424.
- (59) Mao, J.; et al. Airborne measurement of OH reactivity during INTEX-B. *Atmos. Chem. Phys.* **2009**, *9*, 163–173.
- (60) US EPA Chemical Speciation Network - Parameters Reported to the Air Quality System (AQS); <https://www.epa.gov/amtic/chemical-speciation-network-parameters-reported-air-quality-system-aqs> (Accessed: 28th April 2023).
- (61) Kang, C. M.; Koutrakis, P.; Suh, H. H. Hourly Measurements of Fine Particulate Sulfate and Carbon Aerosols at the Harvard–U.S. Environmental Protection Agency Supersite in Boston. *J. Air Waste Manage. Assoc.* **2010**, *60*, 1327.
- (62) Schroder, J. C.; et al. Sources and Secondary Production of Organic Aerosols in the Northeastern United States during WINTER. *J. Geophys. Res. Atmos.* **2018**, *123*, 7771–7796.
- (63) Zhang, J.; et al. The Response of Summertime Organic Aerosol Composition to Emission Controls in the Northeastern United States. *J. Geophys. Res. Atmos.* **2022**, *127*, e2022JD037056.
- (64) Aiken, A. C.; et al. O:C and OM/OC ratios of primary, secondary, and ambient organic aerosol with high-resolution time-of-flight aerosol mass spectrometry. *Environ. Sci. Technol.* **2008**, *42*, 4478–4485.
- (65) Zhang, Q.; Worsnop, D. R.; Canagaratna, M. R.; Jimenez, J. L. Hydrocarbon-like and oxygenated organic aerosol in Pittsburgh: insights into sources and processes of organic aerosol. *Atmos. Chem. Phys.* **2005**, *5*, 3289–3311.
- (66) Canagaratna, M. R.; et al. Chase Studies of Particulate Emissions from in-use New York City Vehicles. *Aerosol Sci. Technol.* **2004**, *38*, 555–573.
- (67) Arey, J.; et al. Dicarbonyl products of the OH radical-initiated reaction of a series of aromatic hydrocarbons. *Environ. Sci. Technol.* **2009**, *43*, 683–689.
- (68) Zaytsev, A.; et al. Mechanistic study of the formation of ring-retaining and ring-opening products from the oxidation of aromatic compounds under urban atmospheric conditions. *Atmos. Chem. Phys.* **2019**, *19*, 15117–15129.
- (69) Zhang, X.; et al. Influence of vapor wall loss in laboratory chambers on yields of secondary organic aerosol. *Proc. Natl. Acad. Sci. U. S. A.* **2014**, *111*, 5802–5807.
- (70) Ma, P. K.; et al. Evaluating the impact of new observational constraints on P-S/IVOC emissions, multi-generation oxidation, and chamber wall losses on SOA modeling for Los Angeles. *CA. Atmos. Chem. Phys.* **2017**, *17*, 9237–9259.
- (71) Dai, S.; et al. Chemical and stable carbon isotopic composition of PM<sub>2.5</sub> from on-road vehicle emissions in the PRD region and implications for vehicle emission control policy. *Atmos. Chem. Phys.* **2015**, *15*, 3097–3108.
- (72) Wu, X.; et al. Characterization and source apportionment of carbonaceous PM<sub>2.5</sub> particles in China - A review. *Atmos. Environ.* **2018**, *189*, 187–212.
- (73) Cao, F.; et al. New insights into the sources and formation of carbonaceous aerosols in China: Potential applications of dual-carbon isotopes. *National Science Review* **2017**, *4*, 804–806.
- (74) Ulbrich, I. M.; Canagaratna, M. R.; Zhang, Q.; Worsnop, D. R.; Jimenez, J. L. Interpretation of organic components from Positive Matrix Factorization of aerosol mass spectrometric data. *Atmos. Chem. Phys.* **2009**, *9*, 2891–2918.
- (75) Ulbrich, I. M.; Handschy, A.; Lechner, M.; Jimenez, J. L. AMS Spectral Database; <http://cires.colorado.edu/jimenez-group/AMSsd/> (Accessed: 6th June 2023).